Electric field control and optical signature of entanglement in quantum dot molecules

Gabriel Bester and Alex Zunger

National Renewable Energy Laboratory, Golden, Colorado 80401, USA
(Received 1 July 2005; published 25 October 2005)

The degree of entanglement of an electron with a hole in a vertically coupled self-assembled dot molecule is shown to be tunable by an external electric field. Using atomistic pseudopotential calculations followed by a configuration interaction many-body treatment of correlations, we calculate the electronic states, degree of entanglement, and optical absorption. We offer a way to spectroscopically detect the magnitude of electric field needed to maximize the entanglement.

I. INTRODUCTION

A pair of quantum dots or a "quantum dot molecule" (QDM) occupied by two electrons[1,2] or by an electron-hole pair[3] have been offered[1–3] as a basis for quantum computing. The fundamental requirement for such a quantum algorithm is the availability of entangled states and the ability to entangle and disentangle the quantum bits (qubits). In the context of a dot molecule, an entangled electron-hole pair can be represented by the the maximally entangled Bell state $e_T h_T + e_B h_B$, where e and h stand for the electron and the hole (the two qubits) and T and B for their localizations in top or bottom dot. The original proposal[3] and subsequent experiments[3–5] for entangled electron-hole pairs in QDMs promised a *high* degree of entanglement[3] based on analysis via simple models. However, later theoretical work showed[6] that electron-hole entanglement is generally low in such cases and develops a sharp maximum only at a specific interdot separation that critically depends on the size difference of the two dots. Unfortunately, it has proven to be difficult to experimentally control so precisely the interdot distance and the size difference of the two dots. The question we address here is whether the degree of entanglement can be maximized by other means, more accessible experimentally than a variation of the interdot separation. We propose and quantify theoretically that it is possible to *tune* and control the degree of entanglement by applying an external electric field in the growth direction.[7–10] The use of electric field has been demonstrated in quantum dots[7–10] and very recently in a single quantum dot molecules.[11,12] We predict that, while the entanglement at zero field is generally low (35% for our case), it can reach a high value (75% in our case) at a specific electric field $F_{S\,\mathrm{max}}$. Moreover, precisely at this field the first two exciton lines merge, giving a well-defined spectroscopic signature of the point of maximum entanglement.

II. METHOD

In order to obtain reliable results for the correlated exciton states, it is of foremost importance to accurately account for the multiband character of the hole states and for the correct strain dependence in the coupling region (between the dots), as demonstrated in Refs. 6 and 13. We have thus solved the pertinent Schrödinger equation atomistically, in a multiband fashion. We use the Hamiltonian

$$H = -1/2\nabla^2 + \sum_{\alpha,n} v_\alpha(\mathbf{r} - \mathbf{R}_n) + V_{\mathrm{SO}} + |e|Fz \qquad (1)$$

under an external electric field F applied in [001] (z) direction. The atomistic pseudopotentials v_α of atom of type α and the nonlocal spin-orbit potential V_{SO} are fit to reproduce InAs and GaAs bulk properties.[6,14] The atomic positions $\{\mathbf{R}_n\}$ are obtained by minimizing the atomistic strain energy (via valence force field[15]) for a given shape and size of the dots. The single-particle Hamiltonian is diagonalized in a basis

$$\Psi = \sum_{n,k} A_{n,k} \phi_{n,k} \qquad (2)$$

of pseudopotential Bloch functions $\phi_{n,k}$ as outlined in Ref. 16, thus permitting coupling of various Bloch states. Correlations are treated via a many-body expansion in Slater determinants[17,18] where the electrons not included dynamically are represented by a model screening of the Coulomb and (long and short range) exchange.[19] The entanglement is calculated according to the von Neumann entropy of entanglement[13,20]

$$S(\Psi) = -\mathrm{Tr}\,\rho_A \log_2 \rho_A = -\mathrm{Tr}\,\rho_B \log_2 \rho_B, \qquad (3)$$

where ρ_A is the reduced density matrix for qubit "A" (the electron) and ρ_B is the reduced density matrix for qubit "B" (the hole). The density matrices are calculated from the *correlated* CI exciton density which requires a projection of the exciton wave functions on the dot localized basis set.[13] Our quantum dots have a truncated cone shape (12 nm base and 2 nm height) with a composition ranging from pure InAs at the top to $In_{0.5}Ga_{0.5}As$ at the base, as determined in Ref. 3. The interdot separation, defined as the wetting layer separation of both dots, is fixed at 7.9 nm. We wish to emphasize that the numerical values of the electric field where certain effects occur (anticrossing of levels or maximum entanglement) depends on the size and geometry of the dots so the specific values of fields should be taken only as illustrations.

III. SINGLE-PARTICLE PICTURE
FOR THE DOT MOLECULE

The bonding (b) and antibonding (a) electron molecular levels of a dot molecule will be denoted as E_a, E_b. For an idealized (mostly unrealistic) symmetric case the lowest en-
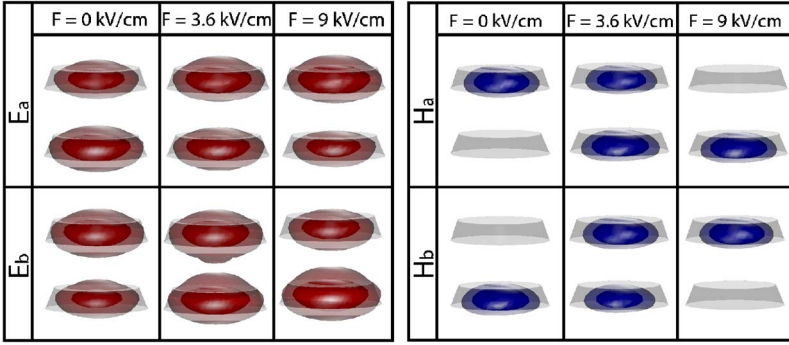
FIG. 1. (Color online) Square of the first two electron and first two hole wave functions of an InGaAs/GaAs quantum dot as a function of electric field at an interdot separation $d=7.9$ nm.

ergy molecular orbitals (MOs) develop from single-dot electron states e_T and e_B located on the bottom (B) and top (T) dots

$$\psi[E_b] = \frac{1}{\sqrt{2}}(e_T + e_B), \quad \psi[E_a] = \frac{1}{\sqrt{2}}(e_T - e_B), \quad (4)$$

and similarly for the holes H_a, H_b. As shown previously,[6,21] in reality, because of strain and random-alloy fluctuations, one does not have a *symmetric* bonding-antibonding behavior even if the dot molecule is made of identical (but nonspherical) dots. This is seen in Fig. 1 where both electron and hole molecular orbital wave functions are shown for zero electric field $F=0$. We see that the (lighter-mass) electrons tunnel between dots, forming bonding-antibonding states as in Eq. (4), but the (heavier-mass) holes remain localized on the top (bottom) dot for the bonding (antibonding) MO $H_b(H_a)$. In Ref. 13 we showed that this inhibited hole tunneling is created by a strain-induced repulsive barrier for the heavy-hole component of the wave functions. The single-particle molecular orbital energy levels are shown in Fig. 2. As we apply an electric field the molecular levels that develop from the single-dot orbitals exhibit anticrossings. The anticrossings show a much stronger tunneling for the electrons than for the holes. We have indicated in Fig. 2 the major character of the molecular states E_a, E_b, H_a, H_b in terms of the localization on individual dots (e_T, e_B, h_T, and h_B) using the calculated MO wave functions of Fig. 1. We see
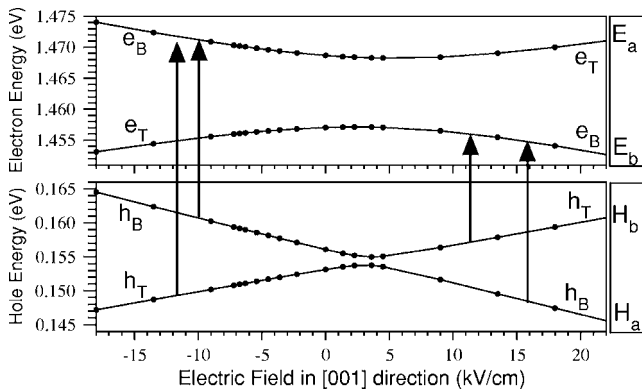

FIG. 2. Single particle electron (upper panel) and hole (lower panel) eigenvalues as a function of electric field for $d=7.9$ nm with respect to the GaAs valence band maximum. We indicate the localization of the MOs on top and bottom dot by e_T, e_B, h_T, h_B.

that for holes at positive fields $\psi(H_a) \simeq h_B$ and $\psi(H_b) \simeq h_T$ while for electrons $\psi(E_a) \simeq e_T$ and $\psi(E_b) \simeq e_B$. The opposite is true for negative fields. Thus, by applying an electric field we can tune the localization of the MO's and, for instance, compensate for size, composition or shape differences of both dots. We will see that this tuning of localization will also control the degree of entanglement.

IV. OPTICAL TRANSITIONS: FROM THE SINGLE-PARTICLE TO MANY-BODY PICTURE

There are four possible transitions between the four molecular levels shown as vertical arrows in Fig. 2. Their single-particle transition energies $\varepsilon_g^{i,j}$ (differences between the energies from Fig. 2) are given in Fig. 3(a) and show maxima and minima vs field. We note in Fig. 3(a) the character of the four transitions in terms of localization on single-dot orbitals. We see that at high fields, the lowest—and highest-energy transitions involve wave function localization on *different* dots: for example E_bH_b is e_Bh_T at positive fields, and e_Th_B at negative fields. Thus, the corresponding dipole transitions are expected to be weak ("dark states"). In contrast the second and third transitions at high fields involve the *same* dots: for example, E_bH_a is e_Bh_B at positive fields and e_Th_T at negative field. Thus, the corresponding dipole transitions are expected to be large ("bright states").

The single-particle approximation underlying Fig. 3(a) is valid only in the case of large fields, where e-h Coulomb effects are small compared to the field-driven variation in the single-particle levels. At these large fields, the excitons are pure Slater determinants with localization on either e_Th_T or e_Th_B or e_Bh_T or e_Bh_B and therefore show no entanglement. We will next see that in the interesting region of electric fields, e-h Coulomb interactions are crucial. In Fig. 3(b) we show the calculated electron-hole Coulomb interaction

$$J_{e,h}[i-j] = \int \int \frac{\psi_i^\star(\mathbf{r}_a)\psi_j^\star(\mathbf{r}_b)\psi_j(\mathbf{r}_b)\psi_i(\mathbf{r}_a)}{\epsilon(\mathbf{r}_a,\mathbf{r}_b)|\mathbf{r}_a - \mathbf{r}_b|} d\mathbf{r}_a d\mathbf{r}_b \quad (5)$$

between the MOs ($i=E_a$ or E_b) and ($j=H_a$ or H_b) using the model of Resta[19] for the screening ϵ. Once again we give the character of the MO states ($E_aH_a, E_aH_b, E_bH_a, E_bH_b$) at large fields in terms of the dot-localized basis (e_Th_T, e_Th_B, e_Bh_T and e_Bh_B). Note that this analysis only applies to the large field region whereas in the intermediate field region, where the different Coulomb integrals are of similar magnitude, the
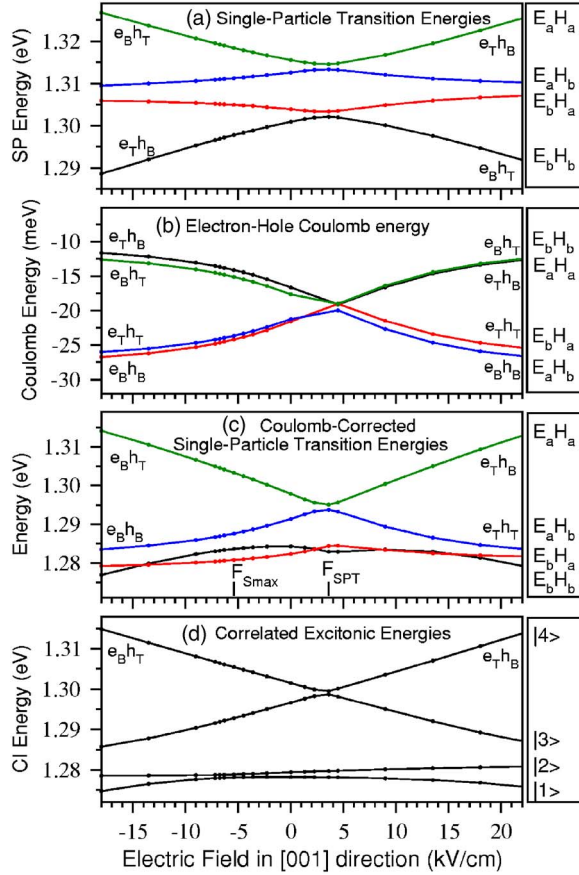
FIG. 3. (Color online) Transition energies for $d=7.9$ nm as a function of electric field in different approximations. (a) Single particle transition energies ε_g. (b) Direct electron-hole Coulomb matrix elements between MOs $J_{e,h}$. (c) Transition energies including electron-hole Coulomb interaction $\varepsilon_g^{i,j}+J_{e,h}^{i,j}$, but without correlation effects. (d) Final correlated exciton results. The bidot products ($e_T h_T$, etc.) are given whenever the MO states (given on the right) are strongly dominated by one of these products. The position of the single-particle tuning field F_{SPT}, where the single-particle wave functions are equally distributed over both dots, and the maximum entanglement field $F_{S\,\mathrm{max}}$ are marked in panel (c).

electron and hole wave functions are delocalized over both dots. This interaction $J_{e,h}$ [Fig. 3(b)] shows the reverse behavior vs field compared with the MO energies ε_g vs field [Fig. 3(a)]. For example, whereas $J_{e,h}[E_b H_b]$ is *maximal* (less negative) at large positive or negative fields, and *minimal* at intermediate fields, the MO band gap $\varepsilon_g[E_b H_b]$ is *minimal* at large positive or negative fields and *maximal* at intermediate fields. Not surprisingly, when one calculates the Coulomb-corrected excitonic transition energy $\varepsilon_g^{i,j}+J_{e,h}^{i,j}$ between the molecular states i and j [Fig. 3(c)] one sees a partial cancellation for the two low-energy transitions, $E_b H_b$ and $E_b H_a$, leading to a weak dependence of the transition energy on field. In contrast, inspection of Figs. 3(a) and 3(b) for the two highest-energy transitions shows that the field dependence of $\varepsilon_g^{i,j}$ and $J_{e,h}^{i,j}$ *reinforce* each other, so the excitonic gap $\varepsilon_g^{i,j}+J_{e,h}^{i,j}$ [Fig. 3(c)] has an *amplified* dependence on field. We conclude that the combination of ε_g and $J_{e,h}$ brings the lowest-energy transitions *closer* to each other, while pushing

the two higher-energy transitions *apart*. This will affect the correlation coupling between the MO's, as seen next.

The Coulomb-corrected excitonic transition energies $\varepsilon_g^{i,j}+J_{e,h}^{i,j}$ neglect the interactions between the different configurations, i.e., the states from Fig. 3(c) are not allowed to combine to form more favorable lower-energy correlated states but are artificially kept as pure $E_a H_a$, $E_a H_b$, $E_b H_a$, or $E_b H_b$ states. This mixing of states (or interaction of configurations) is included in the next step via a configuration interaction (CI) (Refs. 17 and 18) calculation in which we include all Coulomb and exchange integrals from the first four electron and first four hole states (including spin). The results are shown in Fig. 3(d) as a function of electric field. The lowest energy transitions (excitons $|1\rangle$ and $|2\rangle$) have a very weak dependence on field, similarly to the case without correlations [Fig. 3(c)]. However, in contrast to the perturbative approach of Fig. 3(c) the states do not cross but anticross at $F_{S\,\mathrm{max}}$ and have slightly lower energy in the intermediate field region. Both of these observations are expected from a correlated picture where the states acquire additional variational freedom through the ability to mix configurations. Similarly, the states $|3\rangle$ and $|4\rangle$ anticross at F_{SPT} but in a more abrupt fashion. The character of the MO states is now mixed in almost the entire region of fields studied and will be described in the next section in detail.

V. ANALYSIS OF THE CONFIGURATION INTERACTION RESULTS IN A DOT LOCALIZED PICTURE

To understand the correlated CI results we next analyze $|1\rangle,|2\rangle,|3\rangle,|4\rangle$ by decomposing the correlated excitonic states into sums of products of single-dot states $e_T h_T$, $e_B h_T$, $e_T h_B$, and $e_B h_B$ called "bidot products" (see Ref. 13 for details). The results of this decomposition are given in Fig. 4 for states $|1\rangle$ to $|4\rangle$ as a function of the electric field. The vertical axis gives the occupation probability of each of the four possible bidot product as a different curve marked with squares, circles, triangles up, and down for $e_T h_T$, $e_B h_B$, $e_T h_B$, and $e_B h_T$, respectively. For instance, exciton $|1\rangle$ at large positive field shows that it has both the character of a one-center exciton (or "direct exciton") where both particle reside in the same dot ($e_T h_T$) as well as the character of a two-center exciton (or "indirect exciton") where both particles reside on different dots ($e_B h_T$). Figure 5 shows the degree of entanglement calculated for the correlated CI wave functions using the von Neumann formula[6,20] from Eq. (3). The degree of entanglement is shown as a function of electric field for all four excitons as four different curves. The entanglement shows a broad maximum at $F_{S\,\mathrm{max}}$ for the first two excitons $|1\rangle$ and $|2\rangle$ and a sharp maximum at F_{SPT} for the excitons $|3\rangle$ and $|4\rangle$. When a state is made solely of a single bidot product such as $e_B h_T$ it is unentangled, but when it is made of a coherent superposition, such as $e_B h_B \pm e_T h_T$, it might be entangled.

A. Situation at large fields

In the case of very strong positive fields the single-particle picture dominates and both Coulomb and correlation
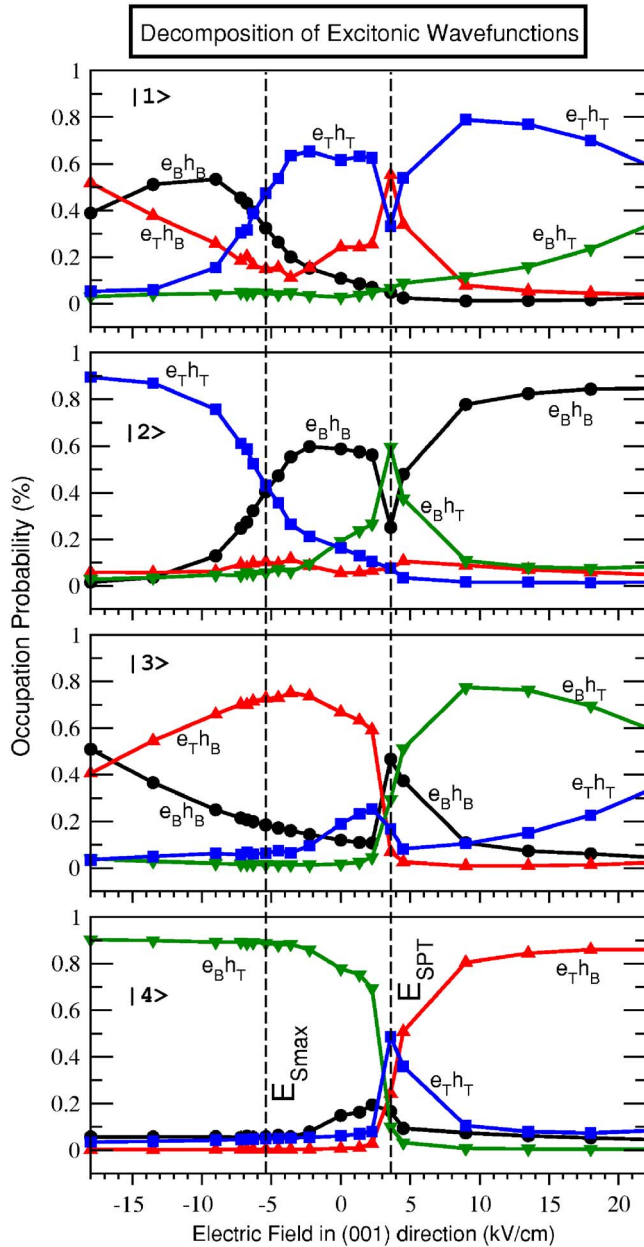
FIG. 4. (Color online) Occupation probabilities given as the bidot products $e_T h_T$ or $e_T h_B$ or $e_B h_T$ and $e_B h_B$ as a function of the electric field for the first four exciton states $|1\rangle$ (a), $|2\rangle$ (b), $|3\rangle$ (c), and $|4\rangle$ (d) for $d=7.9$ nm.

effects become negligible. At these fields, the lowest energy state $|1\rangle$ is purely $e_B h_T$, as the field pulls the electron to the bottom dot and the hole to the top dot. Accordingly, the highest energy state $|4\rangle$ is composed of the energetically less favorable configuration, i.e., having the electron in the top dot and the hole in the bottom dot. This is simply the quantum confined Stark effect where the linear term proportional to the permanent electron-hole dipole moment dominates and hence the excitonic energy follows the field almost linearly. The energy of the intermediate states $|2\rangle,|3\rangle$ have a weak dependence on field and are composed of the remaining $e_T h_T$ and $e_B h_B$ components. Since our quantum dots are intrinsically not symmetric, the electric field at which the state fol-
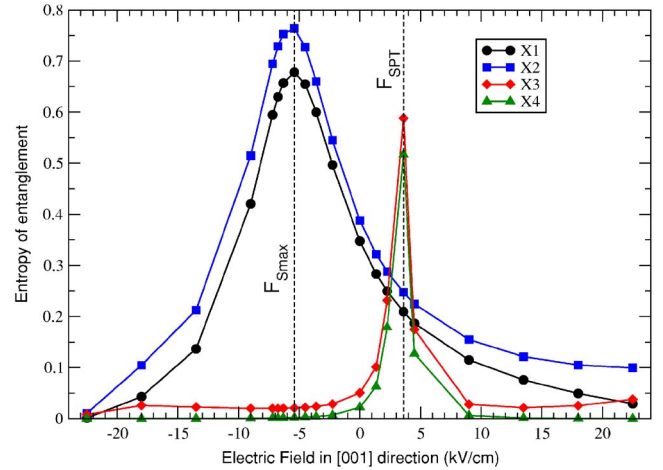

FIG. 5. (Color online) Entropy of entanglement for the first four exciton states as a function of electric field applied along the [001] direction.

low the pure "high-field" regime is different for states $|2\rangle$, $|3\rangle$. We see that state $|2\rangle$ has already above 10 kV/cm almost pure $e_B h_B$ character and an almost constant field dependence [see Fig. 3(d)] while state $|3\rangle$ is still heavily mixed and strongly field dependent around 20 kV/cm. The entanglement of the states $|1\rangle$ and $|4\rangle$ at large fields must be zero because the states are forced into one single configuration (either $e_T h_B$ or $e_B h_T$). The exciton states $|2\rangle$ and $|3\rangle$ can, even at very large fields, form combinations of $e_T h_T$ and $e_B h_B$ configurations with nonzero entanglement. However, any asymmetry between the dots will favor one of these configurations and lower the entanglement of these states.

B. Situation at F_{SPT} where single-particle states are symmetric

At zero field, the electrons build bonding/anti-bonding combinations but are not fully symmetric/antisymmetric (see Fig. 1): localization of the wave function on the top dot is slightly preferred by electrons while the occupation of the bottom dot is preferred by holes (the bonding hole state H_b is nearly entirely localized on the bottom dot). This is mainly because of random alloy fluctuations that make the dots dissimilar (a size difference of the dots, as present in most experimental settings, will create additional asymmetry in the molecular orbital). The holes are mainly localized on the top *or* the bottom dot with strain favoring the bottom dot (Fig. 1). It is, however, possible to restore the symmetry of the electron and hole states by applying an electric field. At the "single-particle tuning" field F_{SPT} (3.6 kV/cm for our dots) the symmetry of the electron and hole molecular orbitals is partially restored (the hole states remain slightly symmetry broken, see Fig. 1). At this single-particle tuning field, F_{SPT} the electron (hole) states are pulled to the bottom dot, just enough to compensate for the zero-field imbalance originating form random alloy fluctuations and strain effects. In the occupation probabilities of Fig. 4 the two excitons $|3\rangle$ and $|4\rangle$ show a heavy mixture of all configurations at F_{SPT}. In Fig. 5 we can see that this combination has a high degree of entanglement of around 60%. However, as we will see in the

next section, the states $|3\rangle$ and $|4\rangle$ are optically nearly dark at F_{SPT} so that entanglement stored in these states will probably be of less interest.

C. Situation at $F_{S\,max}$, where the entanglement is maximized

The entanglement of $|1\rangle$ and $|2\rangle$ (Fig. 5) reaches its maximum of around 75% at $F_{S\,max}$ (-5.4 kV/cm for our dots). At this field the exciton states $|1\rangle$ and $|2\rangle$ are mainly composed of $e_T h_T \pm e_B h_B$ configurations, as shown in Fig. 4, with some contributions from $e_T h_B$ for $|1\rangle$. The entanglement (Fig. 5) as well as the occupation probabilities (Fig. 4) for the excitons $|1\rangle$ and $|2\rangle$ change smoothly when the field is swept from 0 to -20 kV/cm, making a tuning feasible. This is in contrast to the case of high entanglement in $|3\rangle$ and $|4\rangle$ that happens abruptly at F_{SPT}. Note that in order for the e-h entanglement given for $|1\rangle$ and $|2\rangle$ at $F_{S\,max}$ to be useful in a quantum computation scheme, the qubits need to be physically separated to be addressed individually. One possibility for such a separation seems to be the use of *in plane* electric fields that would coherently drive the electron and hole to different neighboring quantum dots. This would constitute the next experimental challenge.

VI. CALCULATION OF THE OPTICAL SPECTRUM AND THE OPTICAL SIGNATURE OF ENTANGLEMENT

The calculated excitonic states of Fig. 3(d) are now used to calculate the absorption spectra in Fig. 6. In Fig. 6 the oscillator strength is plotted for different values of the electric field as a function of the transition energy. The plot shows a total of four transitions marked with $|1\rangle,|2\rangle,|3\rangle,|4\rangle$. Since the transitions $|3\rangle$ and $|4\rangle$ are weak, their position is marked by solid and open arrows respectively. Our calculations include the effect of electron-hole exchange that results in the fine-structure of the exciton.[22] So each of the four exciton lines is actually a quadruplet split by the very small (in the absense of magnetic field) fine-strucutre splittings. We do not focus on the fine-structure in the present contribution (albeit present in the calculaitons) and label the 16 states as four quartets $|1\rangle,|2\rangle,|3\rangle,|4\rangle$. The transitions $|1\rangle$ and $|2\rangle$ have a weak dependence on field and show an anticrossing at $F_{S\,max}$. Transitions $|3\rangle$ and $|4\rangle$ have a strong dependence on field and show an anticrossing at F_{SPT}. The spectra show that at $F_{S\,max}$ the lowest energy exciton $|1\rangle$ becomes dark and progressively gains oscillator strength as the field increases away from the anticrossing. The point of merging of $|1\rangle$ and $|2\rangle$ at
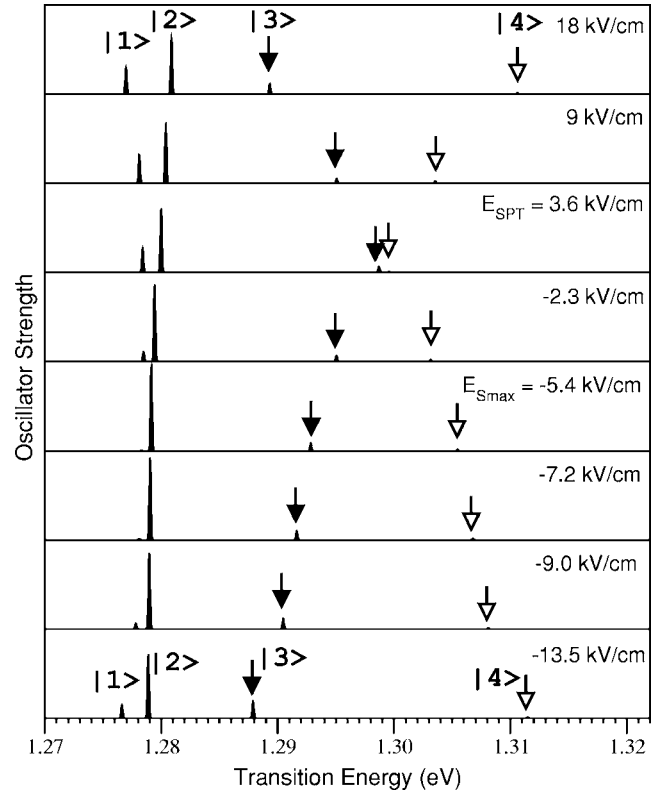

FIG. 6. Oscillator strength of the first four transitions (first 16 transitions including spin) as a function of electric field. The single particle tuning field F_{SPT} and the field of maximum entanglement F_{Smax} are marked. The arrows are merely a guide to the eye for the weak transitions $|3\rangle$ and $|4\rangle$.

the field $F_{S\,max}$ reflects a "resonant conditions" with maximum entanglement (Fig. 4). The distinct spectroscopic signal of the anticrossing (where the lowest line progressively looses oscillator strength) occurs at the point of maximum entanglement and, we suggest, can give experimentalists a simple way to control a delicate quantity such as entanglement.

VII. A SIMPLIFIED MODEL FOR THE RESONANT CONDITION OF ENTANGLEMENT

The physics underlying the resonant condition, that produces the high degree of entanglement in $|1\rangle$ and $|2\rangle$, is revealed in Fig. 7 using the more intuitive basis of dot-
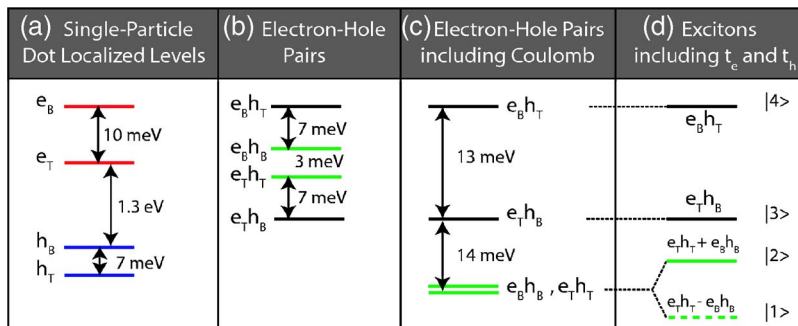

FIG. 7. (Color online) Formation of the highly entangled excitonic states at the critical field $F_{S\,max}$ (-5.4 kV/cm). (a) Single particle electron and hole levels in the dot-localized basis. (b) Simple differences between the single particle electron and hole energies from (a). (c) Adding electron-hole direct Coulomb interaction to (b). (d) Adding electron and hole hopping the the levels from (c).

localized orbitals (as opposed to MO's). To obtain dot-localized orbitals, we rotate the MO's (that are delocalized over both dots) until the on-site Coulomb interaction is maximized.[21,23] This transformation yields single-particle energies of the dot-localized orbitals, denoted as e_T, e_B, h_T, and h_B in Fig. 7(a). Figure 7(a) shows that at $F_{S\,max}$ the energies of the dot-localized electron and hole orbitals are separated by 10 and 7 meV, respectively, with a gap of 1.3 eV. Generally, the energy separation between e_T and e_B and between h_T and h_B can reflect size, composition or shape differences of the two dots. These differences can be tuned by the electric field. Figure 7(b) shows the energies of simple products of these electron and hole states. They show two closely spaced levels (3 meV apart) in the center of the spectrum and two states 7 meV lower and higher in energy. These energies are different from the MO's energies of Fig. 3(a) that are combinations of $e_T h_T$, $e_T h_B$, $e_B h_T$, and $e_B h_B$ at this field and have now the true meaning of an electron (or hole) occupying the top or bottom dot. In the next step, in Fig. 7(c), the two-body Coulomb attraction is taken into account and lowers the $e_T h_T$ and $e_B h_B$ states in such a way that they are about 14 meV below the $e_T h_B$ state. The on-site excitons (both particles in the same dot) separate from the dissociated excitons (electron and hole in different dots) in consequence of a weak e-h binding for the dissociated excitons $e_T h_B$ and $e_B h_T$. Notably, the simple products $e_T h_T$ and $e_B h_B$ are energetically nearly *degenerate* at this level, this is the resonant condition mentioned above. In the last step, in Fig. 7(d), the excitons $|1\rangle$ and $|2\rangle$ are now created by including the effects of electron and hole "hopping" that effectively produce correlated states. Here it is important to realize that our final CI results include all Coulomb and scattering matrix elements and therefore the mechanism labeled here as "tunneling" automatically includes the dipole-dipole coupling known as Förster mechanism. Conceptually, tunneling and Förster coupling are different quantities that can be separated but our anticrossing gap includes both. In Fig. 7(d), the excitons $|1\rangle$ and $|2\rangle$ are forming a bonding-like and antibonding-like combination of the energetically degenerate $e_T h_T$ and $e_B h_B$ states. The excitons $|1\rangle$ and $|2\rangle$ are now split by a small energy of less than 1 meV. This small splitting is conceptually very similar to the Davydov splitting[24] in molecular crystals. The analysis also reveals that $|1\rangle$ is anti-symmetric ($e_T h_T - e_B h_B$) and therefore optically dark while $|2\rangle$ is symmetric ($e_T h_T + e_B h_B$) and optically bright. The high symmetry of these states (purely symmetric and antisymmetric) leads to the high degree of entanglement. Any deviations from $F_{S\,max}$ will lead to a less symmetric combinations as $(1/\sqrt{2})(\alpha e_T h_T + \beta e_B h_B)$ with $\alpha \neq \beta$ with lower entanglement and smaller oscillator strength.

VIII. SUMMARY

We showed that the degree of electron-hole entanglement in coupled quantum dots can be tuned by an external electric field and that the point of maximum entanglement can be identified by measuring the photoluminescence spectra, observing the merging of two peaks. This opens ways for experimentalists to identify the electric field needed to achieve maximum entanglement in specific dot molecules. We finally analyzed the nature of the excitons and revealed the interplay of single particle effects, direct Coulomb binding and electron and hole hopping on the many body levels. We described how these effects conspire to yield a highly entangled state.

[1] D. P. DiVincenzo, Science **270**, 255 (1995).

[2] D. Loss and D. P. DiVincenzo, Phys. Rev. A **57**, 120 (1998).

[3] M. Bayer, P. Hawrylak, K. Hinzer, S. Fafard, M. Korkusinski, Z. R. Wasilewski, O. Stern, and A. Forchel, Science **291**, 451 (2001).

[4] K. Hinzer, M. Bayer, J. P. McCaffrey, P. Hawrylak, M. Korkusinski, O. Stern, Z. R. Wasilewski, S. Fafard, and A. Forchel, Phys. Status Solidi B **224**, 385 (2001).

[5] M. Bayer, G. Ortner, A. Larionov, V. Timofeev, A. Forchel, P. Hawrylak, K. Hinzer, M. Korkusinski, S. Fafard, and Z. Wasilewski, Physica E (Amsterdam) **12**, 900 (2002).

[6] G. Bester, J. Shumway, and A. Zunger, Phys. Rev. Lett. **93**, 047401 (2004).

[7] P. W. Fry, I. E. Itskevich, D. J. Mowbray, M. S. Sloknick, J. J. Finley, J. A. Barker, E. P. O'Reilly, L. R. Wilson, I. A. Larkin, P. A. Maksym, M. Hopkinson, M. Al-Khafaji, J. P. R. David, A. G. Cullis, G. Hill, and J. C. Clark, Phys. Rev. Lett. **84**, 733 (2000).

[8] I. Shtrichman, C. Metzner, B. D. Gerardot, W. V. Schoenfeld, and P. M. Petroff, Phys. Rev. B **65**, 081303(R) (2002).

[9] M. Sugisaki, H. W. Ren, S. V. Nair, K. Nishi, and Y. Masumoto, Phys. Rev. B **66**, 235309 (2002).

[10] B. Alen, F. Bickel, K. Karrai, R. Warburton, and P. Petroff, Appl. Phys. Lett. **83**, 2235 (2003).

[11] H. J. Krenner, M. Sabathil, E. C. Clark, A. Kress, D. Schuh, M. Bichler, G. Abstreiter, and J. J. Finley, Phys. Rev. Lett. **94**, 057402 (2005).

[12] G. Ortner, M. Bayer, Y. Lyanda-Geller, T. L. Reinecke, A. Kress, J. P. Reithmaier, and A. Forchel, Phys. Rev. Lett. **94**, 157401 (2005).

[13] G. Bester, A. Zunger, and J. Shumway, Phys. Rev. B **71**, 075325 (2005).

[14] A. J. Williamson, L.-W. Wang, and A. Zunger, Phys. Rev. B **62**, 12963 (2000).

[15] P. N. Keating, Phys. Rev. **145**, 637 (1966).

[16] L.-W. Wang and A. Zunger, Phys. Rev. B **59**, 15 806 (1999).

[17] A. Szabo and N. S. Ostlund, *Modern Quantum Chemistry* (McGraw-Hill, New York, 1989).

[18] A. Franceschetti, H. Fu, L.-W. Wang, and A. Zunger, Phys. Rev.

B **60**, 1819 (1999).

[19] R. Resta, Phys. Rev. B **16**, 2717 (1977).

[20] C. H. Bennett, H. J. Bernstein, S. Popescu, and B. Schumacher, Phys. Rev. A **53**, 2046 (1996).

[21] L. He, G. Bester, and A. Zunger, cond-mat/0503492, Phys. Rev. B. (to be published).

[22] G. Bester, S. Nair, and A. Zunger, Phys. Rev. B **67**, 161306(R) (2003).

[23] C. Edmiston and K. Ruedenberg, Rev. Mod. Phys. **35**, 457 (1963).

[24] D. P. Craig and S. H. Walmsley, *Excitons in Molecular Crystals* (W. A. Benjamin, Inc., New York, 1968).